Monthly Notices of the ROYAL ASTRONOMICAL SOCIETY

MNRAS **474,** 1296–1306 (2018)
Advance Access publication 2017 October 26

doi:10.1093/mnras/stx2786

RoboPol: connection between optical polarization plane rotations and gamma-ray flares in blazars

D. Blinov,[1,2★] V. Pavlidou,[1,3] I. Papadakis,[1,3] S. Kiehlmann,[4] I. Liodakis,[1,5] G. V. Panopoulou,[6] E. Angelakis,[7] M. Baloković,[6] T. Hovatta,[8] O. G. King,[6] A. Kus,[9] N. Kylafis,[1,3] A. Mahabal,[6] S. Maharana,[10] I. Myserlis,[7] E. Paleologou,[1,3] I. Papamastorakis,[1,3] E. Pazderski,[9] T. J. Pearson,[6] A. Ramaprakash,[10] A. C. S. Readhead,[6] P. Reig,[1,3] K. Tassis[1,3] and J. A. Zensus[7]

[1]*Department of Physics and Institute for Theoretical and Computational Physics (ITCP), University of Crete, 71003 Heraklion, Greece*
[2]*Astronomical Institute, St Petersburg State University, Universitetsky pr. 28, Petrodvoretz, 198504 St Petersburg, Russia*
[3]*Foundation for Research and Technology – Hellas, IESL, Voutes, 7110 Heraklion, Greece*
[4]*Owens Valley Radio Observatory, California Institute of Technology, Pasadena, CA 91125, USA*
[5]*KIPAC, Stanford University, 452 Lomita Mall, Stanford, CA 94305, USA*
[6]*Cahill Center for Astronomy and Astrophysics, California Institute of Technology, 1200 E California Blvd, MC 249-17, Pasadena, CA 91125, USA*
[7]*Max-Planck-Institut für Radioastronomie, Auf dem Hügel 69, D-53121 Bonn, Germany*
[8]*Tuorla Observatory, Department of Physics and Astronomy, University of Turku, Väisäläntie 20, FI-21500 Piikkiö, Finland*
[9]*Toruń Centre for Astronomy, Nicolaus Copernicus University, Faculty of Physics, Astronomy and Informatics, Grudziadzka 5, PL-87-100 Toruń, Poland*
[10]*Inter-University Centre for Astronomy and Astrophysics, Post Bag 4, Ganeshkhind, Pune 411 007, India*

Accepted 2017 October 24. Received 2017 October 24; in original form 2017 May 31

ABSTRACT

We use results of our 3 yr polarimetric monitoring programme to investigate the previously suggested connection between rotations of the polarization plane in the optical emission of blazars and their gamma-ray flares in the GeV band. The homogeneous set of 40 rotation events in 24 sources detected by *RoboPol* is analysed together with the gamma-ray data provided by *Fermi*-LAT. We confirm that polarization plane rotations are indeed related to the closest gamma-ray flares in blazars and the time lags between these events are consistent with zero. Amplitudes of the rotations are anticorrelated with amplitudes of the gamma-ray flares. This is presumably caused by higher relativistic boosting (higher Doppler factors) in blazars that exhibit smaller amplitude polarization plane rotations. Moreover, the time-scales of rotations and flares are marginally correlated.

Key words: polarization – galaxies: active – galaxies: jets – galaxies: nuclei – gamma-rays: galaxies.

1 INTRODUCTION

Blazars are a subclass of active galactic nuclei with relativistic jets oriented towards the Earth. Due to the close alignment of jets with the line of sight, their emission is strongly relativistically boosted and prevails in the overall emission (Blandford & Königl 1979). The broad-band spectral energy distribution (SED) of a blazar has two broad humps, peaking in the IR–X-ray bands and in the MeV–TeV band. The low-energy part of the SED is produced by relativistic electrons in the jet emitting synchrotron radiation. The nature of the high-energy component is uncertain. For instance, it is unknown what kind of particles in the jet is responsible for upscattering of photons to gamma-ray energies (Böttcher et al. 2013) and where the gamma-ray emitting site is located in the jet (e.g. Poutanen & Stern 2010; Agudo et al. 2011).

Optical emission of blazars is often significantly polarized owing to its synchrotron origin. Despite the fact that optical fractional polarization is correlated with the total flux in optical and gamma-rays for some blazars (Itoh et al. 2016), ordinarily both the electric vector position angle (EVPA) and fractional polarization behave erratically (Uemura et al. 2010). However, a number of events have been reported, where the EVPA performs continuous and gradual rotations, whose amplitudes are as high as hundreds of degrees. In some cases these EVPA rotations occur together with flares in multiple bands (e.g. Marscher et al. 2010; Aleksić et al. 2014). The physical processes behind the EVPA rotations and their connection to gamma-ray emission of blazars remain unclear. There are a

★ E-mail: blinov@physics.uoc.gr

number of models proposed for the interpretation of such events. They can be divided into two general classes: random walk and deterministic models. The former class explains polarization rotations as occasional periods of smooth variability in EVPA curves produced by stochastic variations of the polarization vector (Jones et al. 1985; Marscher 2014; Kiehlmann et al. 2016). Deterministic models describe EVPA variability by relativistic aberration (Abdo et al. 2010a; Larionov et al. 2013; Aleksić et al. 2014), change of the magnetic field structure (Zhang et al. 2016) or magnetic field reconnections (Deng et al. 2016) or other deterministic processes (Lyutikov & Kravchenko 2017). It has been suggested that both types of EVPA rotations can occur even in a single blazar (Blinov et al. 2015; Kiehlmann et al. 2016).

In order to increase the number of detected EVPA rotations and improve our understanding of this phenomenon we started the *RoboPol* programme.[1] It has been designed for efficient detection of EVPA rotations in a statistically meticulously defined sample of blazars (Pavlidou et al. 2014). Together with monitoring data provided by the Large Area Telescope (LAT) onboard the *Fermi* gamma-ray space observatory (Atwood et al. 2009), it provides an unrivalled opportunity to investigate the potential connection between optical EVPA variability and gamma-ray activity.

RoboPol started observations at Skinakas observatory, Greece, in 2013 May. The EVPA rotations detected during its first 3 yr of operation were presented in Blinov et al. (2015, 2016a,b, hereafter Papers I, II and III). In Paper I, we analysed a set of EVPA rotation events detected during the first observing season and their connection to gamma-ray flaring activity in blazars. We found that it is unlikely that all EVPA rotations are produced by random variability of the polarization plane. Moreover, it is very unlikely that none of the EVPA rotation events are connected with accompanying flares in the gamma-ray band. In this paper, we verify results of Paper I using the entire set of rotation events detected in 3 yr. We search for the existence of correlations between parameters of EVPA rotations and gamma-ray flares. Such correlations are expected if the two classes of events are physically connected.

The values of the cosmological parameters adopted throughout this work are $H_0 = 67.8\,\mathrm{km\,s^{-1}\,Mpc^{-1}}$, $\Omega_\mathrm{m} = 0.308$ and $\Omega_\Lambda = 1 - \Omega_\mathrm{m}$ (Planck Collaboration XIII 2016). In all the statistical tests, we use a limit $p = 0.05$ as the acceptance limit.

2 OBSERVATIONS AND DATA REDUCTION

2.1 Optical observations

The observation routines used for acquisition of the optical data have been described in King et al. (2014) and Paper I. Nevertheless, for reader's convenience, we briefly summarize our observations here. Our polarimetric and photometric measurements were performed using *RoboPol* photopolarimeter, which was specifically designed for the project. The polarimeter is installed at the 1.3 m telescope of the Skinakas observatory.[2] The data analysed in this paper were taken during the 2013–2015 observing seasons. The monitored sample included 62 gamma-ray–loud and 15 gamma-ray–quiet sources. It has been selected on the basis of stringent, objective and bias-free criteria (see Pavlidou et al. 2014, for details). The EVPA rotation events analysed in this paper have been reported in Papers I–III.

All data were obtained with the *R*-band filter. The exposure length was adjusted according to the brightness of each target, which was estimated during the short pointing exposures, depending also on the sky conditions. The data were processed using the specialized pipeline described in detail by King et al. (2014).

The mean value of $E(B-V) = 0.11^\mathrm{m}$ in the fields of our sources, suggests that typical interstellar polarization is less than 1 per cent (Serkowski, Mathewson & Ford 1975). The EVPA is commonly defined with accuracy between 1° and 10°; however it strongly depends on the fractional polarization of the source and its brightness. The polarization degree is typically measured with accuracy better than 1 per cent. A detailed description of the instrument model and error analysis is given in King et al. (2014).

In order to resolve the 180° ambiguity of the EVPA, we followed a standard procedure (see e.g. Kiehlmann et al. 2013), which is based on the assumption that temporal variations of the EVPA are smooth and gradual, hence adopting minimal changes of the EVPA between consecutive measurements. This procedure is described in more detail in Papers I and II.

2.2 Gamma-ray observations

For the acquisition of the gamma-ray data, we closely followed the procedure described in Paper I. We analysed the *Fermi* LAT data. The *Fermi* gamma-ray space observatory observes the entire sky at energies of 20 MeV–300 GeV every 3 h in normal mode (Atwood et al. 2009). We processed the data in the energy range $100\,\mathrm{MeV} \leq E \leq 100\,\mathrm{GeV}$ using the unbinned likelihood analysis of the standard *Fermi* analysis software package Science Tools v10r0p5 and the instrument response function $P8R2\_SOURCE\_V6$. Source class photons (evclass=128 and evtype=3) were selected within a 15° region of interest centred on a blazar. A cut on the satellite zenith angle ($<90^\circ$) was used to exclude the Earth limb background. The diffuse emission from the Galaxy was modelled using the spatial model gll_iem_v06. The extragalactic diffuse and residual instrumental backgrounds were included in the fit as an isotropic spectral template iso_source_v05. The background models[3] include all sources from the 3FGL (third *Fermi*-LAT source catalogue; Acero et al. 2015) within 15° of the blazar. Photon fluxes of sources beyond 10° from the blazar and spectral shapes of all targets were fixed to their values reported in 3FGL. The source is considered to be detected if the test statistic, TS, provided by the analysis exceeds 10, which corresponds to approximately a 3σ detection level (Nolan et al. 2012). The systematic uncertainties in the effective LAT area do not exceed 10 per cent in the energy range we use (Ackermann et al. 2012). This makes them insignificant with respect to the statistical errors that dominate over the short time-scales analysed in this paper. Moreover, our analysis is based on relative flux variations. Therefore, the systematic uncertainties were not taken into account.

Different time bins t_int, from 2 to 25 d were used, depending on the flux density of the object. In order to make the analysis more robust, we increased sampling of the photon flux curves overlapping adjacent time bins. The centres of the bins were separated by $t_\mathrm{int}/4$ interval from each other. This prevents losses of possible short-term events in the light curves and reduces the dependence of results on the particular position of the time bins. The oversampling introduces an autocorrelation in the photon flux curves, which, however, does not affect the results presented in this work (see also Paper I).

[1] http://robopol.org
[2] http://skinakas.physics.uoc.gr/
[3] http://fermi.gsfc.nasa.gov/ssc/data/access/lat/4yr_catalog/gll_psc_v16.xml

3 THE CONNECTION BETWEEN EVPA ROTATIONS AND GAMMA-RAY FLARES

In Paper I, we reported on 16 EVPA rotation events detected in 14 blazars (hereafter 'rotators') during the 2013 observing season and investigated their connection to gamma-ray activity. Later, in Papers II and III, we analysed statistical properties of 24 more rotations detected in 2014 and 2015. In the following sections, we extend the analysis of Paper I to the entire set of 40 EVPA rotations detected in 24 blazars (see table A1 in Paper III) and investigate whether these events are related to the gamma-ray flaring activity of the blazars.

3.1 Time lags between rotations and gamma-ray flares

We identify gamma-ray flares according to a formal definition of a gamma-ray flare similar to the one proposed by Nalewajko (2013): 'a flare is a contiguous period of time, associated with a given photon flux peak, during which the photon flux exceeds 2/3 of the peak value, and this lower limit is attained exactly twice – at the start and at the end of the flare'.

We searched for gamma-ray flares within time intervals corresponding to *RoboPol* observing seasons of each blazar. The flares are marked by the red points in the photon flux curves of rotators shown in Figs 1–3. Then we fitted these events using profiles with an exponential rise and decay. This kind of profile is commonly used for fitting individual blazar flare pulses in optical, gamma and radio bands (e.g. Abdo et al. 2010b):

$$F(t)=F_{\rm c}+\sum_{i=1}^{N}F_{\rm p,i}\left(\exp\left(\frac{t_{\rm p,i}-t}{T_{\rm r,i}}\right)+\exp\left(\frac{t-t_{\rm p,i}}{T_{\rm d,i}}\right)\right)^{-1}. \quad (1)$$

$F_{\rm c}$ represents the constant photon flux level underlying the flares, N is the number of flares, $F_{\rm p,i}$ measures the amplitude of the ith flare, $t_{\rm p,i}$ describes the time of the peak (it corresponds to the actual maximum only for symmetric flares), and $T_{\rm r,i}$ and $T_{\rm d,i}$

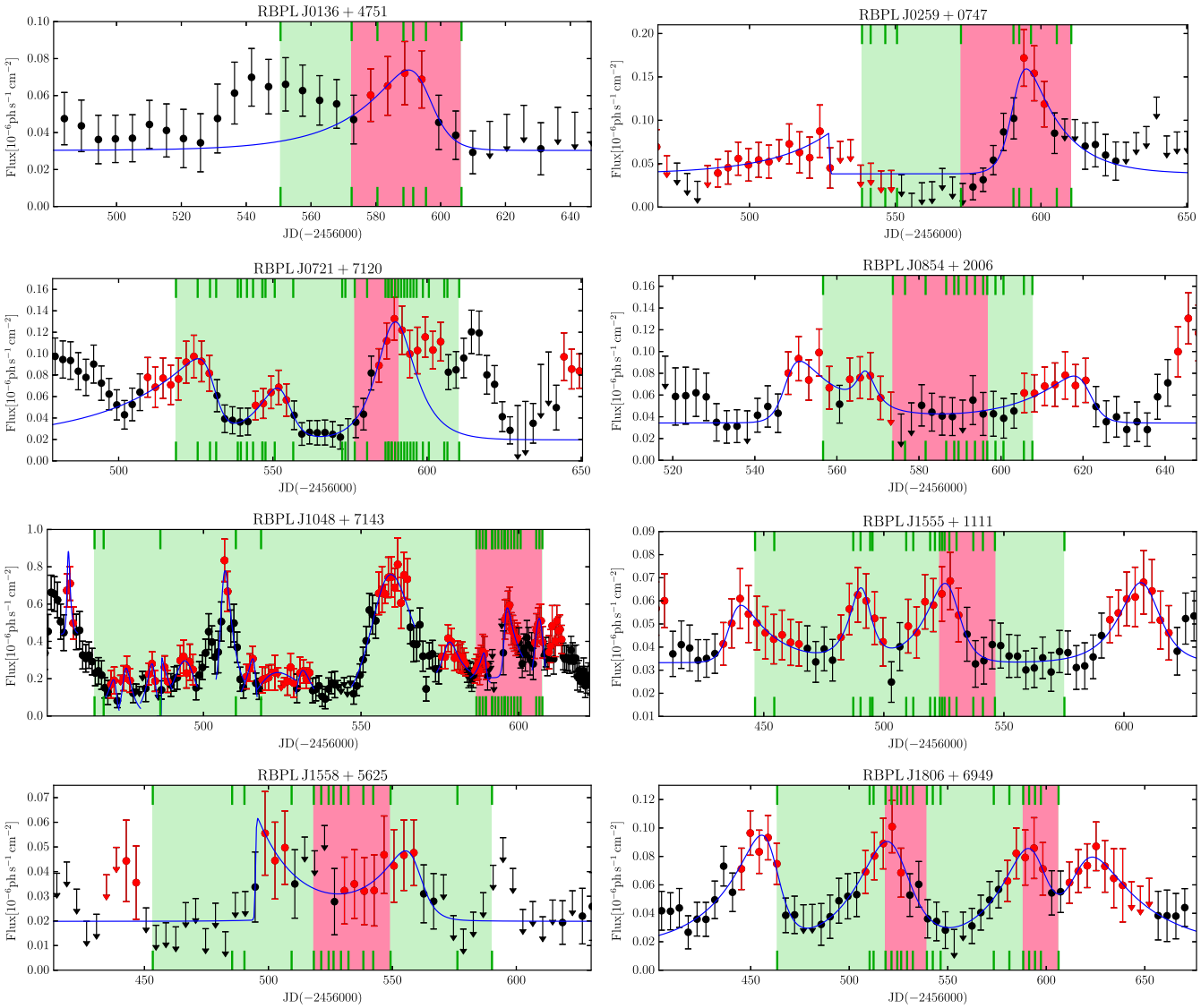

Figure 1. Gamma-ray light curves of objects with detected rotations of EVPA during the 2013 *RoboPol* observing season. The season interval is marked by the green (light) area. The pink (dark) area shows duration of the rotation. Green ticks mark moments of our optical EVPA measurements. The red points (light grey in black and white renderings of the figures) indicate intervals identified as flares. The points are separated by $t_{\rm int}/4$. The blue line is the best least-squares fit of equation (1) to the data.

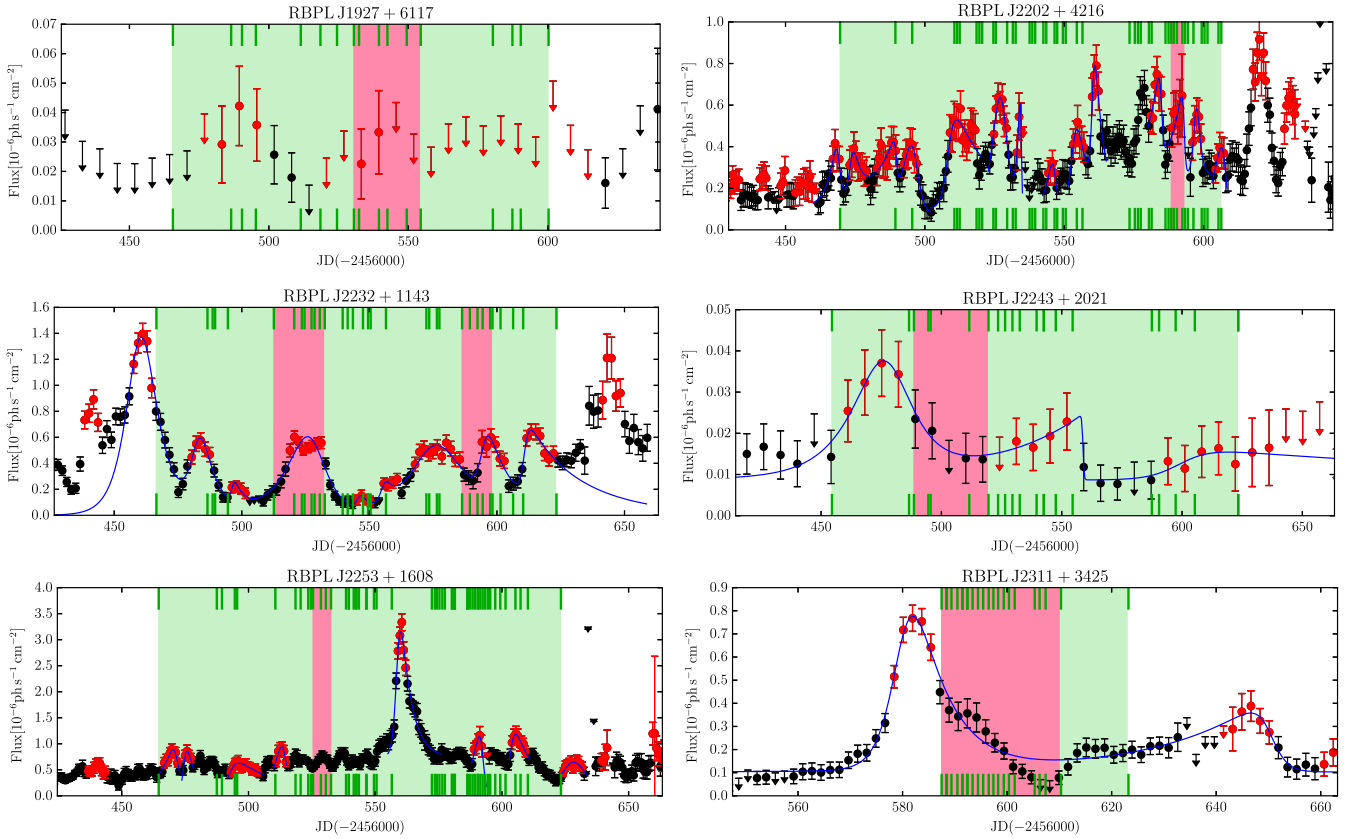

Figure 1 – *Continued*

measure the rise and decay time, respectively. All the parameters were set to be free during the fitting procedure, while initial values used in the fitting procedure were estimated from the photon flux curves. The flares in RBPL J1927+6117 from the 2013 season and RBPL J1809+2041 and RBPL J1836+3136 from the 2015 season could not be fitted due to the poor sampling of the photon flux curves. In most of the cases, all flares identified along the observing season were fitted together using equation (1). However, in several cases (e.g. 2014 curves for RBPL J1512-0905 and RBPL J1800+7828), a decent fit could not be achieved for all flares together or it resulted in physically meaningless values of parameters (e.g. negative fluxes). In these curves, we fitted each gamma-ray flare separately. The best fits of the curves are shown by the blue lines in Figs 1–3.

Time lags, $\tau_{\rm obs}$, between rotations and the closest gamma-ray flares were estimated as $\tau_{\rm obs} = \overline{T^{\rm rot}} - t_{\rm p}$, where $\overline{T^{\rm rot}}$ is the middle point of each EVPA rotation, defined as the mean Julian Date (JD) of the first and the last points of the rotation. Fig. 4 shows the distribution of time lags. The distribution has a clear peak around zero time lag. The mean of the distribution is 1.5 d, while the standard deviation is 19 d. The Kolmogorov–Smirnov (K-S) test rejects the hypothesis that the distribution is consistent with the uniform distribution at the 0.4 per cent confidence level. At the same time, the distribution is consistent with the normal distribution (p-value = 0.03) according to normality test by D'Agostino & Pearson (1973).

3.2 Observed gamma-ray flare amplitudes versus time lags

In Paper I, we found that high-amplitude gamma-ray flares are concurrent in time with EVPA rotations, while some low-amplitude flares have time lags that are significantly different from zero. We investigate the existence of this trend with the full set of detected EVPA rotations. Following the analysis of Paper I, we normalized the amplitude, $F_{\rm p}$, of the gamma-ray flare closest to the EVPA rotation event by the average photon flux, $F_{\rm 3FGL}$, of each blazar as listed in 3FGL. The relative amplitudes versus the time lags are plotted in Fig. 5. The filled black squares show redshift-corrected time lags i.e. $\tau_{\rm corr} = \tau_{\rm obs}/(1+z)$, while open symbols represent blazars with either unknown or uncertain z (see Paper III for the list of redshifts). The distribution of points in Fig. 5 shows possible bimodality along the amplitude axis, which suggests existence of two classes of flares: high and low amplitude. Following Paper I, we arbitrarily set the limit between the two classes at $F_{\rm 3FGL}/F_{\rm p} = 5$. The apparent tendency for the difference of time lags between these high- and low-amplitude flares, reported in Paper I, remained for the full set of rotations. All eight brightest flares in Fig. 5, located above the dashed line, are consistent with $\tau_{\rm corr} = 0$. At the same time, there are a number of low-amplitude flares which appear to have non-zero time lags with respect to EVPA rotations.

However, we must examine the statistical significance of this apparent difference. The mean time lag, $\overline{\tau_{\rm corr}}$, for the high- and low-amplitude samples is 4.2 and −1.9 d. According to the Student's t-test, the null-hypothesis of identical mean values is accepted (p-value = 0.21). A similar conclusion holds for absolute values of $\tau_{\rm corr}$. The standard deviation of time lags, $\sigma_{\tau_{\rm corr}}$, for the high- and low-amplitude samples is 6.1 d and 11.8 d. According to tests for equality of variances by Levene (1960) and Bartlett (1937), we cannot reject the null-hypothesis that the standard deviations are equal (p-value = 0.51 and 0.11). Based on these results, we conclude that $\overline{\tau_{\rm corr}}$ and $\sigma_{\tau_{\rm corr}}$ for the high- and low-amplitude flares are consistent

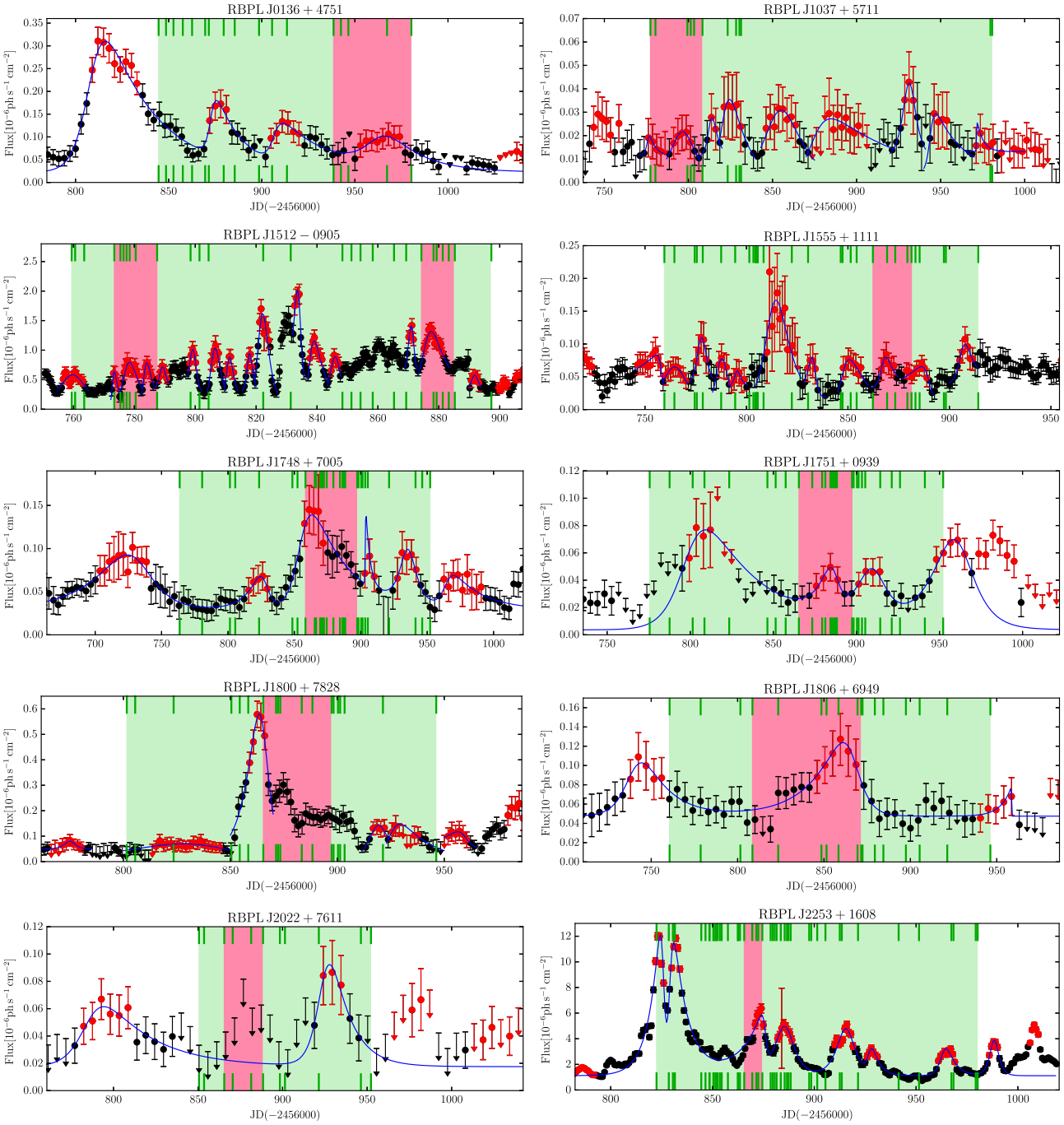

Figure 2. Same as Fig. 1 for the 2014 observing season.

with being equal. Hence, the apparent distinction between high- and low-amplitude flares in Fig. 5 is statistically insignificant.

3.3 Are all time lags consistent with zero?

The results from the analysis in Section 3.2 suggest that $\overline{\tau_{\rm corr}}$ is the same for the high- and low-amplitude gamma-ray flares. Although the distributions of $\tau_{\rm corr}$ in the two groups are sparsely sampled, it appears possible that the two are identical. The larger scatter of $\tau_{\rm corr}$ in low-amplitude flares may be attributed to experimental noise, the effects of which are more pronounced in the case of light curves with low photon counts.

To investigate this effect for each of the gamma-ray light curves, we computed the ratio $N_{\rm up}/N_{\rm det}$, where $N_{\rm det}$ is the number of points with detected photon flux (i.e. TS $>$ 10) and $N_{\rm up}$ is the number of determined upper limits. Both numbers only refer to the time range corresponding to the *RoboPol* observing season of each blazar. In Fig. 6, we show the distribution on the $\tau_{\rm corr}$–$F_{\rm p}/F_{\rm 3FGL}$ plane, where the size of points is proportional to $N_{\rm up}/N_{\rm det}$. This figure suggests that points with larger time lags between rotations and flares tend to also have larger fraction of non-detections in the

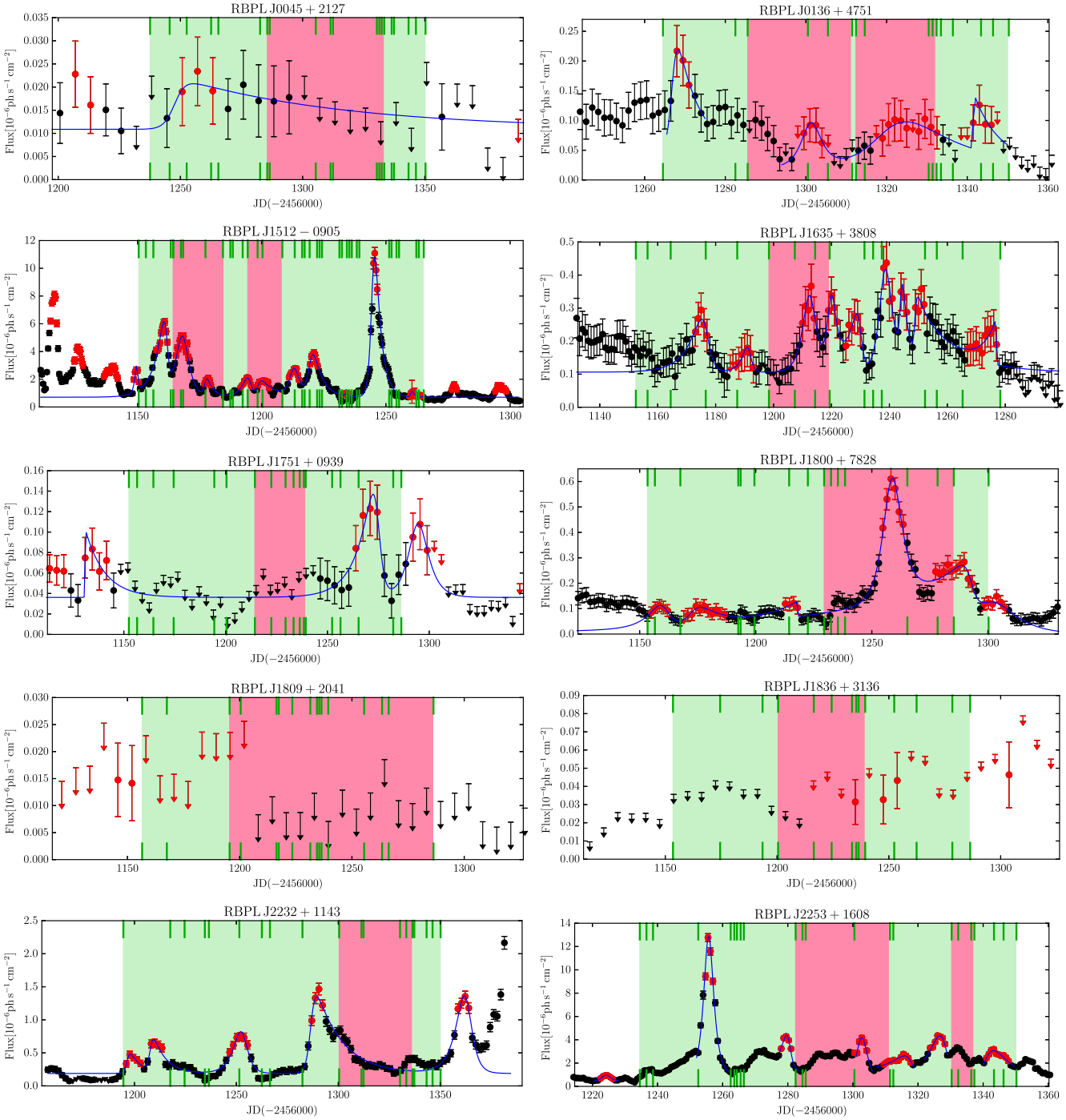

Figure 3. Same as Fig. 1 for the 2015 observing season.

gamma-ray photon flux curves. In fact, the Pearson's correlation coefficient for $|\tau_{\rm corr}|$ and $N_{\rm up}/N_{\rm det}$ is 0.58 (p-value $= 2 \times 10^{-4}$). As a result, the time lags in some cases may not be real, as the gamma-ray flare truly associated with the EVPA is not sampled due to low statistics of data points with significant flux detection.

Furthermore, we compared current data with those used in Paper I, where the *Fermi*-LAT Pass 7 data were analysed with the previous version of Science Tools v9r33p0, and the photon fluxes were normalized with average fluxes of blazars from the 2FGL catalogue (Nolan et al. 2012). The difference between 2FGL and 3FGL is that the latter has a number of improvements in the analysis. For instance, it uses better model of the diffuse Galactic and isotropic emissions as well as more accurately characterized instrument response functions. Also the 3FGL catalogue incorporates data from twice longer time span than 2FGL. However, we did not find any systematic difference in photon fluxes for our sample of rotators between the two catalogues. Moreover, these values are strongly correlated ($r = 0.998$) and the slope of the best-fitting line in the $F_{\rm 3FGL}$ versus $F_{\rm 2FGL}$ plane is consistent with unity. Fig. 7 shows the difference between Pass 7 and Pass 8 data normalized with

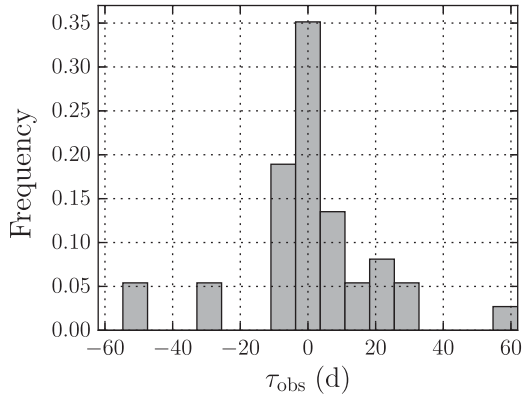

Figure 4. Distribution of observed time lags, $\tau_{\rm obs}$, between the *RoboPol* EVPA rotations and the *Fermi* gamma-ray flares.

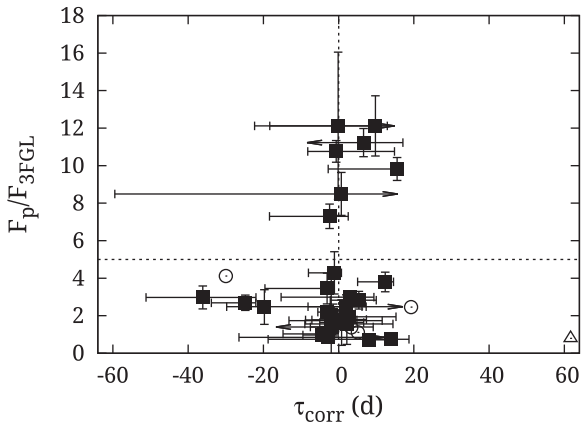

Figure 5. Normalized gamma-ray flare amplitude, $F_{\rm p}/F_{\rm 3FGL}$, versus time lags, $\tau_{\rm corr}$. Filled squares, open circles and triangles correspond to well-defined, uncertain and unknown redshift. For the last category, we use $\tau_{\rm obs}$. The horizontal dashed line indicates $F_{\rm p}/F_{\rm 3FGL} = 5$, where we put the border between high- and low-amplitude flares.

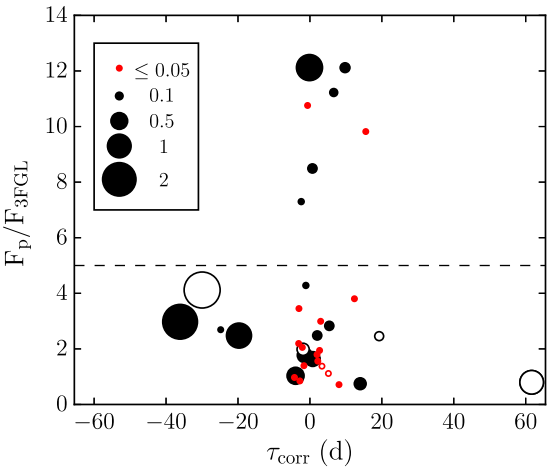

Figure 6. Time lags, $\tau_{\rm corr}$, versus normalized gamma-ray flare amplitude, $F_{\rm p}/F_{\rm 3FGL}$. The size of the points indicates $N_{\rm up}/N_{\rm det}$ – the fraction of the *RoboPol* observing season when the photon flux of the rotator was lower than the *Fermi* LAT detection limit. Open symbols represent events in blazars with uncertain or unknown redshift.

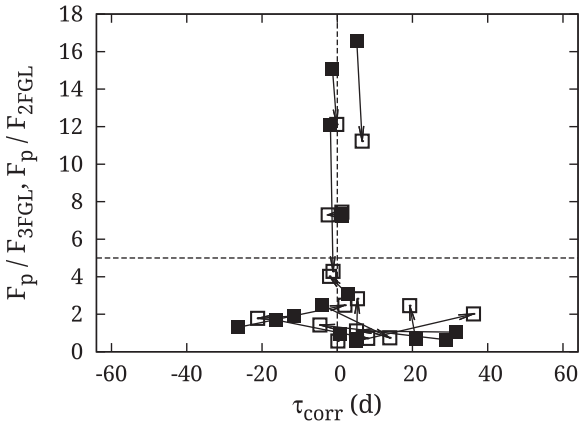

Figure 7. Time lags, $\tau_{\rm corr}$, versus normalized gamma-ray flare amplitude, $F_{\rm p}/F_{\rm 3FGL}$ (open squares) and $F_{\rm p}/F_{\rm 2FGL}$ (filled squares), for the 2013 season events. For direct comparison with Paper I two other seasons are omitted.

2FGL and 3FGL average photon fluxes. The filled squares represent data from fig. 8 in Paper I and the open squares are the data for corresponding events from this work. The figure shows that high-amplitude flares preferentially changed the relative amplitude between the two versions of the analysis, while low-amplitude events mostly changed the time lag. The mean difference of the time lag for low-amplitude events in the two data sets in Fig. 7 is 16.3 d. It is close to $\sigma_{\tau_{\rm corr}} = 18$ d of the low-amplitude events in Fig. 5. This implies that unaccounted uncertainties mostly affect amplitudes and time lags for high- and low-amplitude events, respectively. In other words, if a gamma-ray flare is strong enough, the position of its peak (and hence $\tau_{\rm corr}$) is not affected by any experimental uncertainties that have not been taken into account by the data analysis procedure. On the other hand, if an EVPA rotation is intrinsically linked with a gamma-ray flare of a small amplitude, then the determination of their time lag will be difficult due to the low-counts statistics, which may prevent the accurate determination of the flare peak.

Based on these arguments, we conclude that the higher apparent spread of time lags between rotations and low-amplitude gamma-ray flares compared to that of high-amplitude events is not necessarily a real effect. Rather, it could be caused by insufficient sampling of the gamma-ray photon flux curves (due to low photon statistics) and the subsequent uncertainties in the determination of the flare parameters. Therefore, Fig. 5 cannot be considered as evidence of two types of EVPA rotations. Our analysis indicates that all EVPA rotations are related to gamma-ray flares with $\overline{\tau_{\rm corr}} = 1.5 \pm 3.1$ d, which (given the uncertainties in our estimate of the beginning and end of a rotation) is fully consistent with zero values i.e. *all EVPA rotations could be simultaneous with gamma-ray flares*.

3.4 Are the time lags random?

The result of Section 3.3 suggests that EVPA rotations happen simultaneously with gamma-ray flares. However, most of the gamma-ray light curves in Figs 1–3 show many flares. Therefore, it is possible that the simultaneity between flares and rotations is accidental and not due to a physical link between the events. In Paper I, we showed that this is highly unlikely. We did this by demonstrating that the cumulative distribution function (CDF) of $|\tau_{\rm corr}|$ can be produced accidentally only with very low probability ($\sim 5 \times 10^{-5}$). In other words, if we randomly 'throw rotations' on the *Fermi*

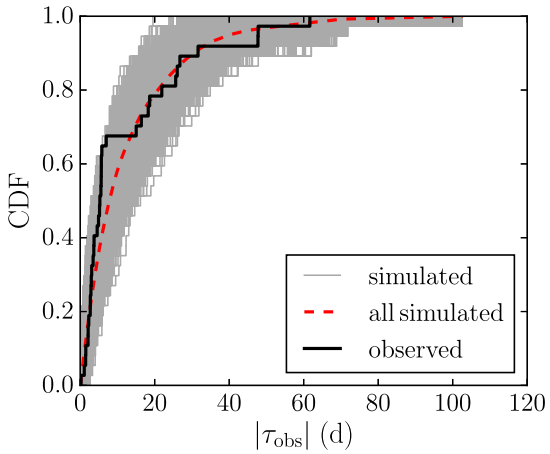

Figure 8. CDFs of the time lags between the EVPA rotations and $t_{\rm p}$ of the closest gamma-ray flares for the main sample rotators. Black line – observed time lags, thin grey lines – 10^4 simulated values for the whole sample of rotations (see the text for details).

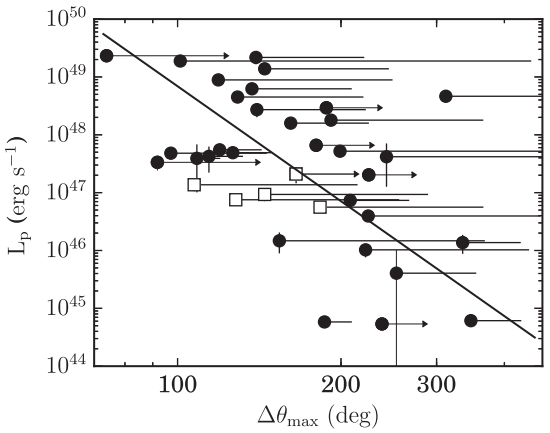

Figure 9. Gamma-ray flare luminosity versus rotation amplitude. The linear fit is shown by the line. Open squares correspond to blazars with uncertain z.

gamma-ray light curves, it is unlikely that we will get as short time lags as we observed.

Here, we conduct a similar analysis using the full three seasons set of EVPA rotations. We used the gamma-ray photon flux curves and the flare fits from Section 3.1. For each of the rotators with defined $\tau_{\rm corr}$, we randomly selected a JD from the uniform distribution within the time range corresponding to the *RoboPol* observing season for this blazar. Then we identified the closest gamma-ray flare to this JD and obtained $\tau_{\rm corr,sim}$ as was done for the observational data. For blazars where two EVPA rotations were observed during a single season, we independently performed this procedure twice. Repeating the experiment 10^6 times we constructed the CDF of $|\tau_{\rm corr,sim}|$ for each trial. In Fig. 8, we show 10^4 of these CDFs (grey lines) together with the observed CDF of $|\tau_{\rm corr}|$ (black). Out of the 10^6 simulated CDFs, only 70 are located in their entirety closer to zero than the observed one (i.e. located to the left of the observed CDF, shown by the black solid line in Fig. 8). This result implies that the probability of *all* time lags in the sample being accidentally so close to zero, as observed, is $\sim 7 \times 10^{-5}$. Thereby, we confirm the results of Paper I, and we conclude that the small time lags we observe suggest a physical link between EVPA rotations and gamma-ray flares.

4 CORRELATIONS BETWEEN PARAMETERS OF EVPA ROTATIONS AND GAMMA-RAY FLARES

The results from the analysis in Section 3 suggest the hypothesis that some (if not all) EVPA rotations must be physically related with the nearest gamma-ray flares. If this is the case, one would expect that at least some properties of these events are correlated. In the following subsections, we discuss the results found in the course of this analysis.

4.1 Flare luminosity versus rotation amplitude

We quantify the amplitude of the gamma-ray flare nearest to an EVPA rotation by the measure $L_{\rm p}$, the gamma-ray luminosity at its peak. The amplitude of the rotation, $\Delta\theta_{\rm max}$, is simply the difference between the maximum and minimum values of EVPA during the rotation. The dependence of $L_{\rm p}$ on $\Delta\theta_{\rm max}$ is plotted in Fig. 9.

Hereafter, we use logarithmic scales because the functional dependence of variables is unknown and it allows us to test the general case of power-law dependence, which also includes linear correlation. The two quantities in Fig. 9 are anticorrelated with $r = -0.54$ (p-value $= 7 \times 10^{-4}$). The best ordinary least-squares bisector (OLSB; Isobe et al. 1990) fit to the data gives the slope value -6.6 ± 1.5, which implies high significance of the correlation.

It should be noted that $\Delta\theta_{\rm max}$ have relatively large uncertainties and in several cases they are defined only as lower limits. These uncertainties are caused by observational restraints, when either start and/or end of a rotation cannot be pinpointed accurately due to insufficient cadence of observations. There is no bias in the values of these uncertainties with respect to blazar properties. For instance, they are not correlated to $\Delta\theta_{\rm max}$ or $L_{\rm p}$. Therefore, we ignore these uncertainties in further analysis for simplicity and omit in figures for better readability.

Any correlation of $L_{\rm p}$ with some other parameter may be a manifestation of one of the following situations: the parameter under consideration may be correlated with the relative flare amplitude, $F_{\rm p}/F_{\rm 3FGL}$, the redshift, z, or the beaming properties of the sources i.e. the Doppler factor, δ. We have not found any significant correlation between $\Delta\theta_{\rm max}$ and $F_{\rm p}/F_{\rm 3FGL}$ ($r = -0.06$, p-value $= 0.72$). However, we indeed found a correlation between δ, z and $\Delta\theta_{\rm max}$, as we discuss below.

4.2 Redshift versus rotation amplitude

In Fig. 10, we show dependence of the redshift on $\Delta\theta_{\rm max}$. The two quantities appear to be anticorrelated ($r = -0.56$ and p-value $= 0.001$ for spectroscopic z), while the OLSB best-fitting line has a highly significant slope -2.3 ± 0.2. The correlation between z and $\Delta\theta_{\rm max}$ can be caused by a physical relation between $L_{\rm p}$ and $\Delta\theta_{\rm max}$, and the fact that our observing sample suffers from the Malmquist bias (i.e. correlation between z and $L_{\rm p}$), since it is a flux limited sample. Alternatively, z and $\Delta\theta_{\rm max}$ can be correlated due to cosmic evolution in the properties of rotations (which would induce the correlation of $L_{\rm p}$ and $\Delta\theta_{\rm max}$, since we tend to see more luminous sources at higher redshifts).

4.3 Jet parameters versus rotation amplitude

Throughout this paper, we use the Doppler factors, δ, derived by Hovatta et al. (2009) from the variability of the total flux density

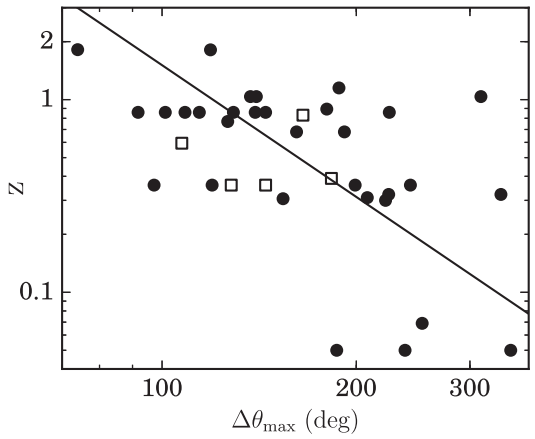

Figure 10. Redshift versus rotation amplitude. The linear fit is shown by the line. Open squares correspond to blazars with uncertain z.

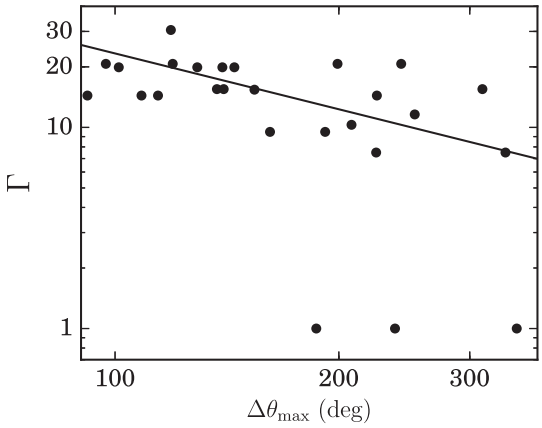

Figure 12. Lorentz factor, Γ, versus rotation amplitude, $\Delta\theta_{\rm max}$. The line is a linear fit in logarithmic scale with the three points at $\Gamma = 1$ excluded.

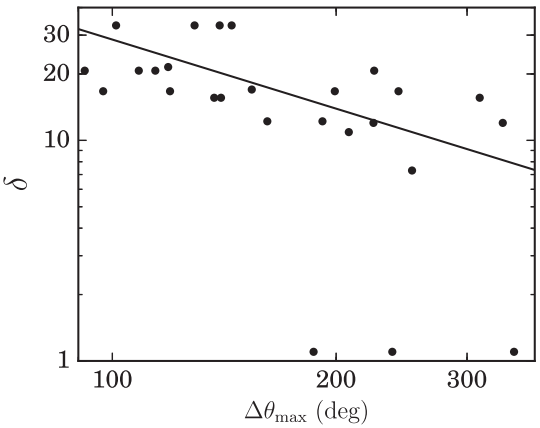

Figure 11. Doppler factor, δ, of a blazar versus rotation amplitude, $\Delta\theta_{\rm max}$. The line is a linear fit in logarithmic scale with the three points of 3C 371 excluded.

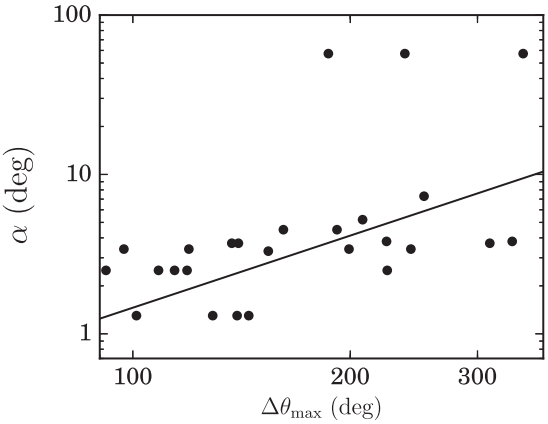

Figure 13. Jet viewing angle, α, versus rotation amplitude, $\Delta\theta_{\rm max}$. The line is a linear fit in logarithmic scale with the three points at $\alpha = 57\overset{\circ}{.}3$ excluded.

at 37 GHz (see table A1 in Paper III). In Fig. 11, we show δ of rotators, as a function of $\Delta\theta_{\rm max}$. It shows a clear anticorrelation of these parameters. This is a surprising result, given the fact that the δ were obtained for an observing period prior to *RoboPol* observations under the assumption of energy equipartition between the magnetic field and the radiating particles (Readhead 1994; Lähteenmäki & Valtaoja 1999). This assumption of equipartition may not hold in all sources (see e.g. Gómez et al. 2016; Bruni et al. 2017). The Doppler factors have on average 30 per cent random errors as shown by Liodakis & Pavlidou (2015). Moreover, δ for the optical emission region may significantly differ from δ of the region emitting at centimetre wavelengths. The three points in Fig. 11 at $\delta = 1.1$, which is approximately order of magnitude lower than others, are rotations in 3C 371 (RBPL J1806+6949). For this source, the Doppler factor in Hovatta et al. (2009) is listed as acceptable, which is their lowest quality class, and the sampling of the source was not very good, which could have resulted in an underestimated Doppler factor (see Liodakis & Pavlidou 2015, for the effects of sampling on the Doppler factor estimates). However, Fan et al. (2013) and Ghisellini et al. (1993) give $\delta = 1.36$ and 0.7 consistent with Hovatta et al. (2009). According to Pesce et al. (2001), this source is an intermediate object between BL Lacs and radio galaxies, which supports the suggestion that the source is less beamed.

When 3C 371 is excluded from the analysis, the correlation coefficient between $\log(\delta)$ and $\log(\Delta\theta_{\rm max})$ is $r = -0.57$ (p-value $= 0.005$), while the slope of the ordinary least-squares bisector regression (Isobe et al. 1990) fit is -1.04 ± 0.03, implying high significance of the correlation.

Additionally, when the gamma-ray luminosity at the flare peak, discussed in the previous subsection, is deboosted as $L_{\rm p,jet} = L_{\rm p}/\delta^4$ (Celotti & Ghisellini 2008) the correlation in Fig. 9 disappears. The correlation coefficient between $L_{\rm p,jet}$ and $\Delta\theta_{\rm max}$ is 0.16 (p-value $= 0.4$).

The Doppler factor depends on the jet viewing angle, α, and the bulk Lorentz factor, Γ, as $\delta = [\Gamma(1 - \beta\cos\alpha)]^{-1}$. Therefore, the correlation between δ and $\Delta\theta_{\rm max}$ can be caused by correlation of the latter with α and/or Γ. We examined both possibilities using the estimates of α and Γ from Hovatta et al. (2009), where they were calculated from δ and apparent jet speeds derived from Very Long Baseline Interferometry observations. The dependences of Γ and α on $\Delta\theta_{\rm max}$ are shown in Figs 12 and 13. Both quantities are marginally correlated with $\Delta\theta_{\rm max}$. The orthogonal distance regression fit of Γ versus $\Delta\theta_{\rm max}$ gives the slope -0.92 ± 0.08, while the correlation coefficient is -0.51 (p-value $= 0.01$). Similarly, the slope in Fig. 13 is 1.5 ± 0.3, $r = 0.51$ (p-value $= 0.01$). The outlying points for 3C 371 were excluded from the analysis in both cases.

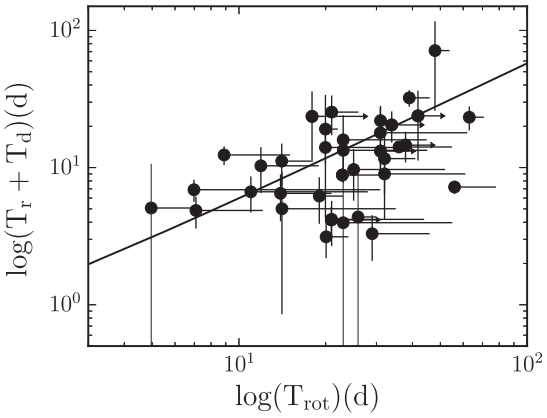

Figure 14. Connection of time-scales of flares and rotations.

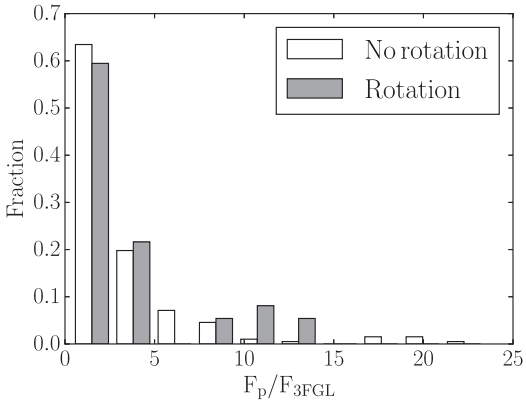

Figure 15. Histogram of relative flare amplitudes for the flares closest to EVPA rotations and all other flares.

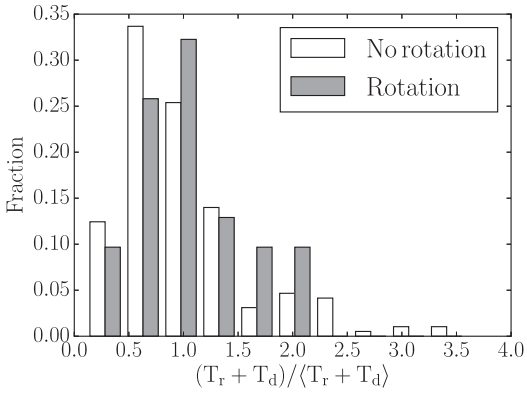

Figure 16. Histogram of normalized time-scales for the flares closest to EVPA rotations and all other flares.

4.4 Correlation of time-scales

In addition to amplitudes, we also find that the durations of the gamma-ray flares and EVPA rotations are correlated. The dependence of the characteristic time-scale of gamma-ray flares, $T_r + T_d$, on the duration, $T_{\rm rot}$ of EVPA rotations is shown in Fig. 14. The two quantities are positively correlated with $r = 0.46$ (p-value $= 0.005$). The slope of the best least-squares fit line 0.57 ± 0.19 implies a correlation significance at the 2.8σ level. Therefore, we conclude that there is a marginal correlation between the time-scales of the detected EVPA rotations and the closest gamma-ray flares. There is a link between the EVPA rotations and gamma-ray flares. However, there are many more gamma-ray flares in the *Fermi* light curves in Figs 1–3, so one may ask whether the flares associated with the EVPA rotations stand out from the rest in any way.

5 ARE THE FLARES ASSOCIATED WITH ROTATIONS PECULIAR?

Visual inspection of the gamma-ray light curves does not reveal any obvious peculiarity of the flares closest to EVPA rotations. In most of the cases, they appear to be similar in amplitude, duration and shape to the rest of the flares occurred during the *RoboPol* observing season. To investigate whether the flares related to EVPA rotations are not segregated in their parameters from other flares, we divided all gamma-ray flares that were identified and fitted in Section 3.1 into two groups with and without associated EVPA rotation events.

In Fig. 15, we show the distribution of relative amplitudes, $F_{\rm p}/F_{\rm 3FGL}$, of the flares for the two groups. The K-S test does not reject the null hypotheses that both samples are drawn from the same parent population (p-value $= 0.86$).

In order to compare the characteristic time-scales of flares in the two groups, we kept only blazars with three or more flares (19 out of 24) and found the average time-scale, $\langle T_r + T_d \rangle$, for each source. Then, we normalized $T_r + T_d$ of each flare by this mean value. The histogram of this quantity for both groups is shown in Fig. 16. According to the K-S test, the two distributions cannot be distinguished (p-value $= 0.26$).

We conclude that gamma-ray flares related to EVPA rotations do not show any peculiar properties. Both amplitudes and durations of the flares accompanied by rotations are statistically similar to those in flares, where no rotation was detected in *RoboPol* data. We emphasize, however, that this analysis is done under the assumption that we detected all EVPA rotations that occurred during our observations. In fact, observational constraints limit the validity of this assumption. The detection efficiency depends on the rotation rate and on the cadence of observations (see section 3.1 of Paper III for details).

6 DISCUSSION AND CONCLUSIONS

In this paper, we investigated the connection between optical EVPA rotations and gamma-ray activity in blazars. We used the data from the *RoboPol* programme i.e. the full 3 yr monitoring and the 40 detected rotations. This is the largest number of rotations detected in a uniform way for a statistically complete sample of blazars so far. The study was possible not only due to *RoboPol* data, but also thanks to the availability of continuous gamma-ray data obtained by *Fermi*-LAT.

In Paper I, based on the analysis of the correlation between the EVPA rotations and gamma-ray flares detected during the first observing season, we had found an indication of a bimodal distribution of $\tau_{\rm corr}$: large amplitude gamma-ray flares appeared to be closely linked with EVPA rotations, while smaller amplitude flares were not. This dependence was considered as a manifestation of two types of rotations coexisting in blazars. In this work, we demonstrated that this difference is caused by the less accurate determination of the flare peak position in the case of flares with low gamma-ray photon statistics.

The major result of our study is that the EVPA rotations are physically linked with gamma-ray flares. We measured the average delay of $\overline{\tau_{\rm corr}} = 1.5 \pm 3.1$ d, which is fully consistent with zero. The uncertainty of $\overline{\tau_{\rm corr}}$ is mainly determined by the uncertainty in the determination of $t_{\rm p}$ of the low-amplitude gamma-ray flares. This uncertainty will not improve significantly in the near future, but the uncertainty of the time lag could be reduced by an increase in the

number of detected EVPA rotations in blazars. We found that the probability that this small time lag between gamma-ray flares and EVPA rotations is accidental and is $\sim 7 \times 10^{-5}$.

This result and the significant correlations we detected between the parameters of the flares and rotations (Section 4), confirm the physical connection between these events. Indeed, we found that both the 'amplitude' and 'duration' of these events are correlated. The significant anticorrelation between the luminosity of the gamma-ray flares and the amplitude of the rotations $\Delta\theta_{\rm max}$ is explained by stronger relativistic boosting in blazars that exhibited lower amplitude EVPA rotations, i.e. when δ is larger (flare luminosity is larger) $\Delta\theta_{\rm max}$ is smaller. This dependence, in turn, is explained by the dependence of $\Delta\theta_{\rm max}$ on the bulk Lorentz factor and the viewing angle of the jet. The faster the jet and the smaller the viewing angle, the lower the amplitude of the rotation. The characteristic time-scale of the gamma-ray flares shows a marginal ($\sim 2\sigma$) positive correlation with the duration of corresponding EVPA rotations: longer gamma-ray flares seem to be associated with longer rotations.

Our results strongly favour the deterministic nature of EVPA rotations. If a substantial fraction of these events was produced by a random walk of the polarization vector, then both amplitudes and time-scales of rotations would be random quantities independent from corresponding properties of gamma-ray flares. In this case the correlations in Figs 9–14 would be smeared out. The connection between parameters of EVPA rotations and gamma-ray flares also implies that these events are produced in the same region of the jet. Therefore, EVPA rotations can be used for localization of the gamma-ray emission zone within the jet. However, the possibility that there is an underlying stochastic process producing a random walk of the polarization vector, superposed with a deterministic process that produces the large rotations contemporaneously with gamma-ray flares, cannot be ruled out based on our data (Kiehlmann et al. 2017). In fact, along with the measurement uncertainties, the presence of random walk events could be responsible for the rather wide spread of points in Figs 9–14.

Finally, we showed that the gamma-ray flares related to EVPA rotations do not show any distinctive properties in their amplitudes or characteristic time-scales when compared to other flares that occurred during *RoboPol* observations. In principle, every gamma-ray flare could be accompanied by an EVPA rotation, and the absence of a recorded rotation in *RoboPol* data could be due to sparse sampling. In order to investigate whether every gamma-ray flare is indeed accompanied by a swing in EVPA, a continuous, very high cadence monitoring of known rotators is required.

ACKNOWLEDGEMENTS

The *RoboPol* project is a collaboration between Caltech in the USA, MPIfR in Germany, Toruń Centre for Astronomy in Poland, the University of Crete/FORTH in Greece and IUCAA in India. The University of Crete group acknowledges support by the 'RoboPol' project, which is implemented under the 'Aristeia' Action of the 'Operational Programme Education and Lifelong Learning' and is co-funded by the European Social Fund (ESF) and Greek National Resources, and by the European Commission Seventh Framework Programme (FP7) through grants PCIG10-GA-2011-304001 'JetPop' and PIRSES-GA-2012-31578 'EuroCal'. This research was supported in part by NASA grant NNX11A043G and NSF grant AST-1109911, and by the Polish National Science Centre, grant number 2011/01/B/ST9/04618. SK is supported by NASA grant NNX13AQ89G. TJP and ACSR acknowledge support from NASA award NNX16AR41G. KT and GVP acknowledge support by the European Commission Seventh Framework Programme (FP7) through the Marie Curie Career Integration Grant PCIG-GA-2011-293531 'SFOnset'. MB acknowledges support from NASA Headquarters under the NASA Earth and Space Science Fellowship Program, grant NNX14AQ07H. We acknowledge the hard work by the *Fermi*-LAT Collaboration that provided the community with unprecedented quality data and made Fermi Science Tools so readily available. We thank members of the *Fermi*-LAT Collaboration for their useful comments that improved the manuscript.

REFERENCES

Abdo A. A. et al., 2010a, Nature, 463, 919
Abdo A. A. et al., 2010b, ApJ, 722, 520
Acero F. et al., 2015, ApJS, 218, 23
Ackermann M. et al., 2012, ApJS, 203, 4
Agudo I. et al., 2011, ApJ, 726, L13
Aleksić J. et al., 2014, A&A, 569, A46
Atwood W. B. et al., 2009, ApJ, 697, 1071
Bartlett M. S., 1937, Proc. R. Soc. A, 160, 268
Blandford R. D., Königl A., 1979, ApJ, 232, 34
Blinov D. et al., 2015, MNRAS, 453, 1669 (Paper I)
Blinov D. et al., 2016a, MNRAS, 457, 2252 (Paper II)
Blinov D. et al., 2016b, MNRAS, 462, 1775 (Paper III)
Böttcher M., Reimer A., Sweeney K., Prakash A., 2013, ApJ, 768, 54
Bruni G. et al., 2017, A&A, 604, A111
Celotti A., Ghisellini G., 2008, MNRAS, 385, 283
D'Agostino R., Pearson E. S., 1973, Biometrika, 60, 613
Deng W., Zhang H., Zhang B., Li H., 2016, ApJ, 821, L12
Fan J.-H., Yang J.-H., Liu Y., Zhang J.-Y., 2013, Res. Astron. Astrophys., 13, 259
Ghisellini G., Padovani P., Celotti A., Maraschi L., 1993, ApJ, 407, 65
Gómez J. L. et al., 2016, ApJ, 817, 96
Hovatta T., Valtaoja E., Tornikoski M., Lähteenmäki A., 2009, A&A, 494, 527
Isobe T., Feigelson E. D., Akritas M. G., Babu G. J., 1990, ApJ, 364, 104
Itoh R. et al., 2016, ApJ, 833, 77
Jones T. W., Rudnick L., Aller H. D., Aller M. F., Hodge P. E., Fiedler R. L., 1985, ApJ, 290, 627
Kiehlmann S. et al., 2013, EPJ Web Conf., 61, 6003
Kiehlmann S. et al., 2016, A&A, 590, A10
Kiehlmann S., Blinov D., Pearson T. J., Liodakis I., 2017, MNRAS, 472, 3589
King O. G. et al., 2014, MNRAS, 442, 1706
Lähteenmäki A., Valtaoja E., 1999, ApJ, 521, 493
Larionov V. M. et al., 2013, ApJ, 768, 40
Levene H., 1960, in Olkin I., Ghurye S., Hoeffding W., Madow W., Mann H., eds, Contributions to Probability and Statistics: Essays in Honor of Harold Hotelling Vol. 2. Stanford University Press, Stanford. p. 278
Liodakis I., Pavlidou V., 2015, MNRAS, 454, 1767
Lyutikov M., Kravchenko E. V., 2017, MNRAS, 467, 3876
Marscher A. P., 2014, ApJ, 780, 87
Marscher A. P. et al., 2010, ApJ, 710, L126
Nalewajko K., 2013, MNRAS, 430, 1324
Nolan P. L. et al., 2012, ApJS, 199, 31
Pavlidou V. et al., 2014, MNRAS, 442, 1693
Pesce J. E., Sambruna R. M., Tavecchio F., Maraschi L., Cheung C. C., Urry C. M., Scarpa R., 2001, ApJ, 556, L79
Planck Collaboration XIII, 2016, A&A, 594, A13
Poutanen J., Stern B., 2010, ApJ, 717, L118
Readhead A. C. S., 1994, ApJ, 426, 51
Serkowski K., Mathewson D. S., Ford V. L., 1975, ApJ, 196, 261
Uemura M. et al., 2010, PASJ, 62, 69
Zhang H., Deng W., Li H., Böttcher M., 2016, ApJ, 817, 63

This paper has been typeset from a TEX/LATEX file prepared by the author.